AIAA xxx
Modular Attitude Guidance Development using the Basilisk Software Framework

Mar Cols Margenet and Hanspeter Schaub

University of Colorado, Boulder, Colorado, 80309, US

Scott Piggott

Laboratory for Atmospheric and Space Physics, Boulder, Colorado, 80309, US

AIAA/AAS Astrodynamics Specialist Conference
September 12–15, 2016 / Long Beach, CA

Modular Attitude Guidance Development using the Basilisk Software Framework

Mar Cols Margenet* and Hanspeter Schaub†
University of Colorado, Boulder, Colorado, 80309, US

Scott Piggott‡
Laboratory for Atmospheric and Space Physics, Boulder, Colorado, 80309, US

A modular attitude reference frame generation architecture is presented that is implemented within the Basilisk astrodynamics software framework. The module nature and message passing interface of Basilisk is exploited to decompose the complex guidance generation process into a series of simpler steps and exchangeable components. Inertial pointing, orbit Hill-frame pointing, orbit velocity-frame pointing and constrained two-body pointing scenarios are considered to generate the base reference frame. Next, additional dynamic reference motion behaviors are super-imposed such as fixed spinning or scanning relative to this base frame. Finally, the last component of the guidance module sequence evaluates the attitude tracking errors required to drive a general body-fixed frame towards the desired reference frame. Numerical simulations illustrate how the individual components can be arranged to yield complex guidance strategies.

I Introduction

Space missions rely highly on the efficiency and reliability of the on-board flight software in order to perform autonomous attitude control or orbit corrections. These critical software functions undergo a stringent review and validation process prior to flight, which can be both costly and time consuming. The Guidance, Navigation and Control (GN&C) blocks are the core of the on-board flight software:

Navigation: The current orientation states and rates of the spacecraft are estimated using absolute and relative measurements. A range of estimation filtering methods are possible that are the focus of ongoing research.[1–5]

Guidance: The desired attitude reference frame that the spacecraft should assume is computed and compared to the current state. Typically, a customized set of software is written to meet mission specific needs and must yield a unique reference frame result.

Control: A concrete control law is implemented to drive the current body frame towards a desired reference frame. Attitude control methods are actively studied, using both linear[6] and nonlinear[7–9] approaches.

While the navigation/estimation and control phases are open in scope and leave room for a range of mathematical strategies, the guidance process is more pragmatic and mission-specific in nature. In the open literature, there is a common lack of documentation on the guidance implementation, indicating that it is commonly developed as an in-house solution. Both reusability and generality of flight software are a milestone to a better management of resources and efforts. Yet, if not done in a very accurate manner that dovetails modularity and flexibility, many hazards threaten to arise, as discussed in Ref. 10. A novel methodology for the attitude reference generation is discussed that is modular and scalable.

*Graduate Student, Aerospace Engineering Sciences, University of Colorado Boulder, AIAA Member

†Alfred T. and Betty E. Look Professor of Engineering, Department of Aerospace Engineering Sciences, University of Colorado, 431 UCB, Colorado Center for Astrodynamics Research, Boulder, CO 80309-0431. AIAA Associate Fellow and AAS Fellow

‡ADCS Integrated Simulation Software Lead, Laboratory for Atmospheric and Space Physics, University of Colorado Boulder, AIAA Member.

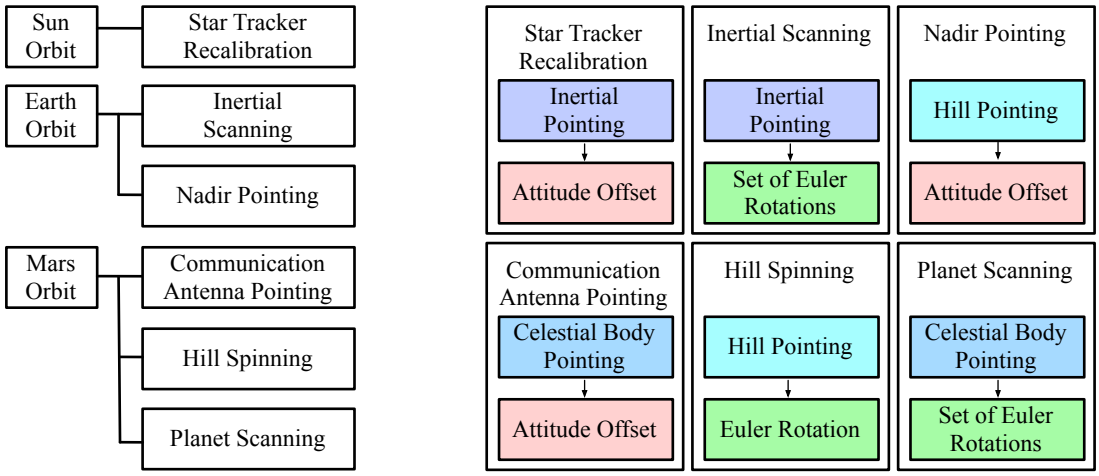

a) Inheritance Guidance Approach **b)** Mix-and-match Guidance Approach

Figure 1: Illustration of Sample Guidance Scenarios.

References 11 and 12 detail a common GN&C setup for space autonomous applications. The navigation, guidance and control functionalities are clearly distinguished as independent processes, and functions from each block are grouped to define several nominal modes. Operational modes generally imply creating an attitude reference about a certain celestial body and driving a determined spacecraft-fixed frame to that reference. The idea in the generalization of the attitude guidance task is to avoid having specific guidance algorithms to fulfill each profile.

Figure 1(a) illustrates a sample guidance design concept based on inheritance. This example considers an Earth-Mars mission with planetary and heliocentric phases. In each phase, a set of final reference states are evaluated through unique algorithms. In contrast, Fig. 1(b) shows how the same guidance scenarios being achieved as a composition of core guidance functionalities. The advantage of fractionating the reference generation is that, for a given set of core modules, a wide variety of guidance behaviors can be achieved through combination.

For example, both a rotation about a hill frame axis and a scanning maneuver across a planet can be performed through constant Euler angle rates relative to a specific pointing attitude. While the pointing nature is, in this case, distinct, the rotational functionality is shared. In other instances it is the pointing reference that is common: pointing a communication antenna towards the Earth and scanning across a planet are both based on a celestial body pointing functionality. Finally, the difference between driving an axis of the main body frame or an alternate spacecraft-fixed component-frame axis, such as the bore-sight of a star tracker, is simply a constant attitude offset.

This paper investigates a methodology to modularize the attitude guidance evaluation into a base reference generation, a dynamic reference generation and a final tracking error evaluation that determines the difference between the reference frame and a particular body-fixed frame. The modular guidance stack is depicted in Fig. 2. Different combinations of pointing and dynamic references yield guidance scenarios of distinct complexity. All proposed guidance schemes are applicable to any type of Keplerian orbit, including elliptic circumnavigation and hyperbolic fly-by trajectories.

Figure 1(b) highlights the sample base pointing references in blue colors; the sample dynamic references are marked in green; the attitude offset present in some tracking error cases is highlighted in red. Within the suggested

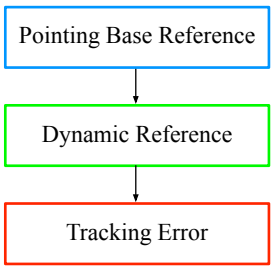

Figure 2: Illustration of the General Guidance Setup.

guidance chain, a Message Passing Interface (MPI) is used to flow the output data from one module into the next. This makes it simple to replace a module in the reference guidance stack with another to change the overall guidance behavior.

Encapsulating the guidance functionalities in completely independent modules instead of monolithic algorithms is a key aspect in terms of software safety. There have been several instances of critical anomalies arising in complex software due to unexpected behavior of commercial off-the-shelf software.[10] With the aim of bringing down mission risks, the suggested staging of independent guidance modules allows scaling up the functionality in a safe and systematic manner. Complexity is built through layers of atomic modules and the decoupling between these units simplifies the verification/validation process because they can be individually tested and analyzed.

The paper is outlined as follows. First, the guidance generation and control setup used throughout the paper are reviewed. An overview of the Basilisk astrodynamics simulation software is presented upon which the proposed guidance solutions are implemented. Then the base reference modes are discussed including inertial pointing, Hill frame pointing, velocity orbit pointing as well as a novel constrained two-body pointing scheme. In the two-body pointing guidance generation, the spacecraft must direct an axis towards a planetary body while pointing a second axis as best as possible at another celestial body. For example, consider pointing a high-gain antenna aligned precisely back at Earth, while rotating the craft to point the solar panel normal as best as possible at the sun. Next the dynamic guidance modes are discussed, which consider spinning about a fixed axis and performing a constant Euler rates maneuver relative to the base reference frame. After developing the underlying mathematics of each module, numerical simulations illustrate the staging strategy to achieve increasingly complex scenarios.

II Problem Statement

II.A Attitude Guidance Behavior

The goal of the GN&C process is to drive a body-fixed frame from its current state $\mathcal{B}$, as estimated by the navigation system, to a final desired reference frame $\mathcal{R}$. Within this process, the guidance block is responsible for generating the desired reference $\mathcal{R}$ and computing the attitude error between the current and desired states.

The computed reference state $\mathcal{R}$ is, in this paper, composed of three parameters: an inertial attitude measure, denoted through the Modified Rodrigues Parameters (MRP) set $\boldsymbol{\sigma}_{R/N}$,[8,13,14] an inertial angular rate vector ${}^{\mathcal{N}}\boldsymbol{\omega}_{R/N}$ expressed in inertial frame $\mathcal{N}$ components, and an inertial angular acceleration vector ${}^{\mathcal{N}}\dot{\boldsymbol{\omega}}_{R/N}$ also in $\mathcal{N}$-frame components. The left-superscript denotes the frame with respect to which the vector components are taken.

This paper assumes a 3-axes attitude control scenario. This assumption is critical when adding base and dynamic reference frame behaviors. Excluded from this scenario are 2-axes attitude control problems where only a single body vector has to be aligned with a reference vector. This is commonly the case of safe-mode sun-pointing operations.

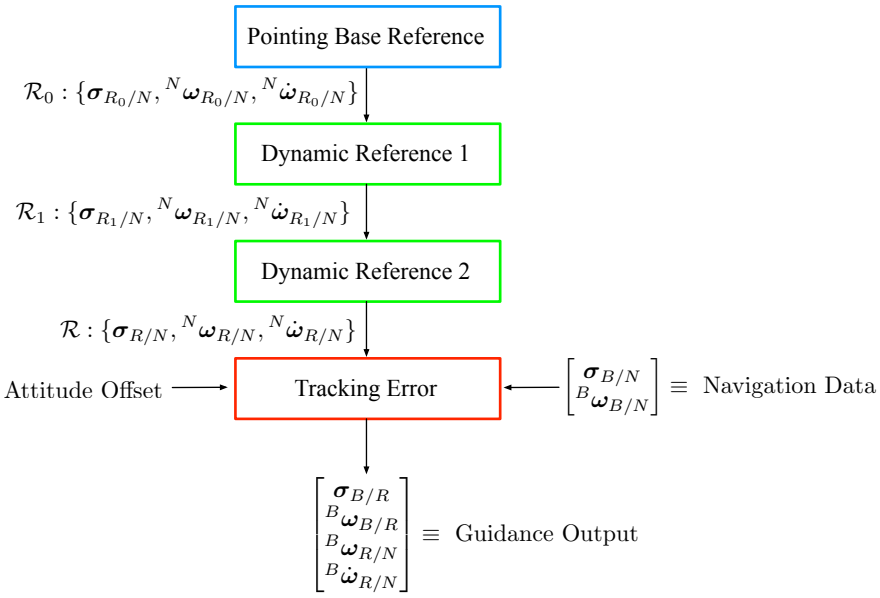

Figure 3: Illustration of the Inputs and Outputs of a Sample Multi-Reference Guidance Chain.

Figure 3 illustrates the flow of inputs and outputs between the cascaded guidance modules. Each data set enters the system only once and is then transferred downstream as necessary. Having a single point of contact with the individual incoming and outgoing data packets avoids redundancy and the conflicts that may arise from it. In this modular guidance stack, the final reference frame is always denoted as $\mathcal{R}$, while the intermediary frames are called $\mathcal{R}_i$. Each stack has a single base guidance module, whose output is $\mathcal{R}_0$. If dynamic guidance modules are included to do spinning or scanning maneuvers, their outputs are denoted as $\mathcal{R}_1$, $\mathcal{R}_2$, etc. While several dynamic guidance modules can be staged one after the other, in this paper only scenarios with a single dynamic module are numerically demonstrated.

The generality of driving any spacecraft-fixed frame to a desired orientation is achieved by maintaining the reference generation completely independent from the knowledge of the body frame. The body frame information is part of the navigation data and it is exclusively used when assessing the current attitude tracking errors.

II.B Attitude Control MRP Feedback

To apply the guidance control, a rigid spacecraft with N Reaction Wheels (RWs) is modelled. The associated differential equations of motion are[8]

$$[I]\dot{\boldsymbol{\omega}}_{B/N} = -[\tilde{\boldsymbol{\omega}}_{B/N}]\left([I]\boldsymbol{\omega}_{B/N} + [G_s]\boldsymbol{h}_s\right) - [G_s]\boldsymbol{u}_s + \boldsymbol{L} \tag{1}$$

where $[I]$ is the spacecraft inertia tensor, $\boldsymbol{L}$ is an external torque and $\boldsymbol{u}_s$ is the set of RW motor torques. The RW spin axis are defined in the $3 \times N$ projection matrix

$$[G_s] = \begin{bmatrix} \hat{\boldsymbol{g}}_{s_1} & \cdots & \hat{\boldsymbol{g}}_{s_N} \end{bmatrix} \tag{2}$$

with $\hat{\boldsymbol{g}}_{s_i}$ being the i^{th} RW spin axis. The $N \times 1$ RW inertial angular momentum matrix $\boldsymbol{h}_s$ is

$$\boldsymbol{h}_s = \begin{bmatrix} J_{s_1}(\boldsymbol{\omega}_{B/N} \cdot \hat{\boldsymbol{g}}_{s_1} + \Omega_1) \\ \vdots \\ J_{s_N}(\boldsymbol{\omega}_{B/N} \cdot \hat{\boldsymbol{g}}_{s_N} + \Omega_N) \end{bmatrix} \tag{3}$$

where J_{s_i} is the RW spin axis inertia.

For the purpose of testing the guidance modules, the following MRP feedback law is implemented that is globally asymptotically stabilizing:[8]

$$[G_s]\boldsymbol{u}_s = K\boldsymbol{\sigma}_{B/R} + [P]\boldsymbol{\omega}_{B/R} - \boldsymbol{\omega}_{R/N} \times ([I]\boldsymbol{\omega}_{B/N} + [G_s]\boldsymbol{h}_s) + [I](\boldsymbol{\omega}_{B/N} \times \boldsymbol{\omega}_{R/N} - \dot{\boldsymbol{\omega}}_{R/N}) + \boldsymbol{L} \tag{4}$$

Here $\boldsymbol{u}_s$ is the control torque being computed, K is the attitude error gain and $[P]$ is the rate error gain matrix. The control block is fed with the guidance output. This information includes the MRP attitude error $\boldsymbol{\sigma}_{B/R}$, the body rate error ${}^{\mathcal{B}}\boldsymbol{\omega}_{B/N}$, the reference rate ${}^{\mathcal{B}}\boldsymbol{\omega}_{R/N}$ and the reference inertial acceleration ${}^{\mathcal{B}}\dot{\boldsymbol{\omega}}_{R/N}$.

III Basilisk Software Architecture

Basilisk is a research and analysis software tool that can be used to study the dynamics and attitude control of spacecraft. It provides a highly flexible and comprehensive open-source simulation framework suitable for both industry and academia.

Basilisk is structured in a way to tie in the efficiency of an object-oriented language such as C++ and the flexible scriptability of Python at the same time. With this purpose, a Python interface is used to set up simulation cases and scenarios. In turn, the computations are driven down to the C/C++ level in order to boost up speed. The different C and C++ modules, each representative of a GN&C algorithm instantiation onboard the spacecraft, interact with each other via an MPI) system that ensures decoupling between the distinct parts of the simulation. Such data flow allows the guidance module setup shown in Fig. 3 to be implemented. The cascading of modules is set at the Python level, allowing different levels of simulation complexity. For example, it is possible to run simulations that include higher order gravitational effects, flexing spacecraft dynamics for both solar panels and fuel slosh, or solar radiation pressure effects. At the same time, basic scenarios emulating only translational or rotational motion can also be configured. It is critical to note that existing C/C++ modules are only loaded to the simulation when they are specifically initialized in the Python layer first. Running each case scenario with only the required modules avoids having unused code in the simulation, which is desired for testability and verification purposes.

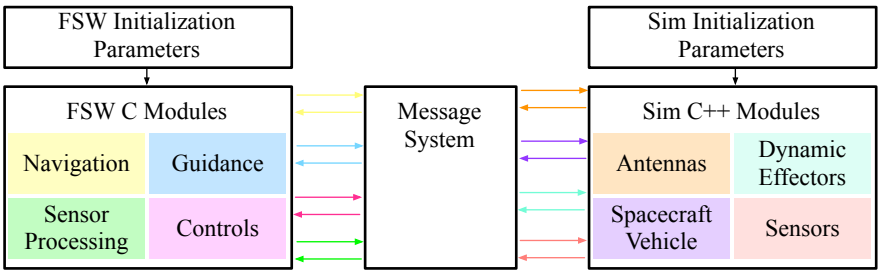

Figure 4: Internal Architecture of Basilisk for a Sample Python Scenario.

The scenario used to test the developed guidance modules includes two processes in a single thread: a dynamics process and a flight software process. In general terms, the dynamics block stands for the simulation of the physical spacecraft, while the flight software (FSW) block emulates the on-board computer functionality. Basilisk is able to simulate a range of sensors, such as rate gyros, star trackers, coarse sun sensors, etc. Navigation modules embed estimation algorithms to predict the various spacecraft states. To easily illustrate the validity of the presented guidance module behaviors, all sensor corruptions are set to zero. Thus, if the reference frame, along with the associate reference rates and accelerations, are properly evaluated, then the control in Eq. (4) will drive the tracking errors asymptotically to zero.

IV Pointing Base Reference Modules

The first guidance stage consists of modules that generate a base pointing reference frame $\mathcal{R}_0$. This attitude frame can be either inertial or non-inertial. The common feature of the base modules is that the generated reference does not depend on any prior frame. Without loss in generality, the reference output inside each module is always labeled as $\mathcal{R}$. If a dynamic reference module is appended to this base module, it is implied that the base module output $\mathcal{R}$ becomes the input reference $\mathcal{R}_0$ of the dynamic one.

IV.A Inertial Pointing

The simplest guidance module is inertial pointing. Here the constant reference frame $\mathcal{R}_0$ is in a general orientation relative to the inertial frame $\mathcal{N}$. The desired inertial orientation is given through a set of constant MRP parameters $\boldsymbol{\sigma}_{R_0/N}$, while the reference frame rates and accelerations are set to zero

$$\boldsymbol{\sigma}_{R/N} = \boldsymbol{\sigma}_{R_0/N} \tag{5a}$$

$$\boldsymbol{\omega}_{R/N} = \dot{\boldsymbol{\omega}}_{R/N} = \mathbf{0} \tag{5b}$$

IV.B Hill- and Velocity-Frame Pointing

The second and third base reference guidance modules are strongly related and developed in a joint manner. Assume the spacecraft is to align with the orbit Hill frame $\mathcal{H} : \{\hat{\imath}_r, \hat{\imath}_\theta, \hat{\imath}_h\}$ or the velocity frame $\mathcal{V} : \{\hat{\imath}_n, \hat{\imath}_v, \hat{\imath}_h\}$. These frames are completely defined by the position and velocity vectors of the spacecraft. The frames $\mathcal{H}$ and $\mathcal{V}$ are each conformed by their own right-handed set of axes where: $\hat{\imath}_r$ is the nadir axis pointing radially outward, $\hat{\imath}_v$ is tangent to the orbit and parallel to the velocity vector, $\hat{\imath}_h$ is defined normal to the orbital plane in the direction of the angular momentum, and finally $\hat{\imath}_\theta$ and $\hat{\imath}_n$ complete their respective right-handed triplet.

Figure 5 illustrates the Hill and velocity frame orientations, each having their origin on the spacecraft location. The inertial frame $\mathcal{N} : \{\hat{\boldsymbol{n}}_1, \hat{\boldsymbol{n}}_2, \hat{\boldsymbol{n}}_3\}$ is also depicted. The inertial position and velocity vectors of the spacecraft

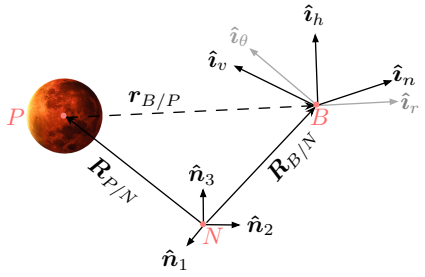

Figure 5: Illustration of the Hill and Velocity Orbit Frames

($\boldsymbol{R}_{B/N}, \boldsymbol{v}_{B/N}$) and the celestial body ($\boldsymbol{R}_{P/N}, \boldsymbol{v}_{P/N}$) are the only variables assumed to be known by the module. The relative position of the spacecraft with respect to the planet $\boldsymbol{r}_{B/P}$ and relative velocity $\boldsymbol{v}_{B/P}$, are obtained through

$$\boldsymbol{r}_{B/P} = \boldsymbol{R}_B - \boldsymbol{R}_P \tag{6a}$$
$$\boldsymbol{v}_{B/P} = \boldsymbol{v}_B - \boldsymbol{v}_P \tag{6b}$$

The Hill $\mathcal{H}$ and velocity $\mathcal{V}$ frame orientations with respect to the inertial frame $\mathcal{N}$ are defined through the following Direction Cosine Matrices (DCMs):

$$[HN] = \begin{bmatrix} {}^{\mathcal{B}}\hat{\boldsymbol{i}}_r{}^T \\ {}^{\mathcal{B}}\hat{\boldsymbol{i}}_\theta{}^T \\ {}^{\mathcal{B}}\hat{\boldsymbol{i}}_h{}^T \end{bmatrix} \qquad [VN] = \begin{bmatrix} {}^{\mathcal{V}}\hat{\boldsymbol{i}}_n{}^T \\ {}^{\mathcal{V}}\hat{\boldsymbol{i}}_v{}^T \\ {}^{\mathcal{V}}\hat{\boldsymbol{i}}_h{}^T \end{bmatrix} \tag{7}$$

where the associated unit direction vectors are defined as:

$$\hat{\boldsymbol{i}}_r = \frac{\boldsymbol{r}_{B/P}}{|\boldsymbol{r}_{B/P}|} \tag{8a}$$
$$\hat{\boldsymbol{i}}_v = \frac{\boldsymbol{v}_{B/P}}{|\boldsymbol{v}_{B/P}|} \tag{8b}$$
$$\hat{\boldsymbol{i}}_h = \frac{\boldsymbol{r}_{B/P} \times \boldsymbol{v}_{B/P}}{|\boldsymbol{r}_{B/P} \times \boldsymbol{v}_{B/P}|} \tag{8c}$$
$$\hat{\boldsymbol{i}}_\theta = \hat{\boldsymbol{i}}_h \times \hat{\boldsymbol{i}}_r \tag{8d}$$
$$\hat{\boldsymbol{i}}_n = \hat{\boldsymbol{i}}_h \times \hat{\boldsymbol{i}}_v \tag{8e}$$

The corresponding Hill orbit and velocity orbit MRP attitude sets are derived from their corresponding DCM.[8]

$$[HN] \to \boldsymbol{\sigma}_{R/N} \qquad \text{or} \qquad [VN] \to \boldsymbol{\sigma}_{R/N} \tag{9}$$

Next, the reference frame rates and accelerations are determined. In the case of the Hill frame $\mathcal{H}$, the angular rate of the reference is that of the orbital motion.

$$\boldsymbol{\omega}_{R/N} = \boldsymbol{\omega}_{H/N} = \dot{f}\hat{\boldsymbol{i}}_h \tag{10a}$$
$$\dot{\boldsymbol{\omega}}_{R/N} = \dot{\boldsymbol{\omega}}_{H/N} = \ddot{f}\hat{\boldsymbol{i}}_h \tag{10b}$$

where f is the true anomaly angle, whose variation is expressed through the following general astrodynamics relation:

$$\dot{f} = \frac{\boldsymbol{r}_{B/P} \times \boldsymbol{v}_{B/P}}{\boldsymbol{r}_{B/P} \cdot \boldsymbol{r}_{B/P}} \tag{11a}$$
$$\ddot{f} = -2\frac{\boldsymbol{v}_{B/P} \cdot \hat{\boldsymbol{i}}_r}{|\boldsymbol{r}_{B/P}|}\dot{f} \tag{11b}$$

The velocity frame $\mathcal{V}$ orientation differs from the Hill frame orientation by a single-axis rotation of angle $-\beta$ in the orbital plane about $\hat{\boldsymbol{i}}_h$, as shown in Fig. 6. The DCM that maps from $\mathcal{H}$ to $\mathcal{V}$ is expressed in terms of the flight path angle β or the classical set of orbital elements as[8]

$$[VH] = \begin{bmatrix} \cos\beta & -\sin\beta & 0 \\ \sin\beta & \cos\beta & 0 \\ 0 & 0 & 1 \end{bmatrix} = \begin{bmatrix} \dfrac{1+e\cos f}{\sqrt{1+e^2+2e\cos f}} & -\dfrac{e\sin f}{\sqrt{1+e^2+2e\cos f}} & 0 \\ \dfrac{e\sin f}{\sqrt{1+e^2+2e\cos f}} & \dfrac{1+e\cos f}{\sqrt{1+e^2+2e\cos f}} & 0 \\ 0 & 0 & 1 \end{bmatrix} \tag{12}$$

The inertial angular rate and acceleration of the velocity frame $\mathcal{V}$ are obtained by

$$\boldsymbol{\omega}_{V/N} = \boldsymbol{\omega}_{V/H} + \boldsymbol{\omega}_{H/N} \tag{13a}$$
$$\dot{\boldsymbol{\omega}}_{V/N} = \dot{\boldsymbol{\omega}}_{V/H} + \dot{\boldsymbol{\omega}}_{H/N} \tag{13b}$$

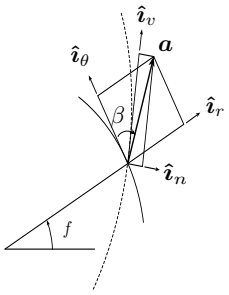

Figure 6: Relationship of the Hill Frame, $\mathcal{H}$, with the Velocity Frame, $\mathcal{V}$.

where

$$\boldsymbol{\omega}_{V/H} = -\dot{\beta}\hat{\boldsymbol{\imath}}_h \tag{14a}$$

$$\dot{\boldsymbol{\omega}}_{V/H} = -\ddot{\beta}\hat{\boldsymbol{\imath}}_h \tag{14b}$$

An analytical expression for β is derived from Eq. (12), whose inertial time derivatives are:

$$\dot{\beta} = \frac{e(e+\cos f)}{1+e^2+2e\cos f}\dot{f}$$

$$\ddot{\beta} = \frac{e(e+\cos f)}{1+e^2+2e\cos f}\ddot{f} + \frac{e(e^2-1)\sin f}{(1+e^2+2e\cos f)^2}\dot{f}^2$$

The velocity-frame base pointing module rates and accelerations are thus defined as

$$\boldsymbol{\omega}_{R/N} = \boldsymbol{\omega}_{V/N} = (\dot{f} - \dot{\beta}\,)\hat{\boldsymbol{\imath}}_h \tag{16}$$

$$\dot{\boldsymbol{\omega}}_{R/N} = \dot{\boldsymbol{\omega}}_{V/N} = (\ddot{f} - \ddot{\beta}\,)\hat{\boldsymbol{\imath}}_h \tag{17}$$

IV.C Constrained Two-Body Pointing

The last base reference module is a novel kinematic solution to a common constrained attitude pointing challenge. A base reference frame $\mathcal{R} : \{\hat{\boldsymbol{r}}_1, \hat{\boldsymbol{r}}_2, \hat{\boldsymbol{r}}_3\}$ is generated that tracks the center of a primary celestial target, e.g. pointing the communication antenna at the Earth, and tries to align the second reference axis towards a second celestial body as best as possible, e.g. pointing a solar panel normal axis to the sun. It is important to note that two attitude conditions in a three-dimensional space compose an overdetermined problem. A TRIAD-like approach is used such that the main constraint is always prioritized over the secondary one.[15]

Figure 7 depicts the desired reference frame $\mathcal{R} : \{\hat{\boldsymbol{r}}_1, \hat{\boldsymbol{r}}_1, \hat{\boldsymbol{r}}_2\}$ and the inertial frame $\mathcal{N} : \{\hat{\boldsymbol{n}}_1, \hat{\boldsymbol{n}}_1, \hat{\boldsymbol{n}}_2\}$. The $\mathcal{R}$ frame has its origin in the spacecraft body $\mathcal{B}$. The points $\mathcal{P}_1$ and $\mathcal{P}_2$ are the primary and secondary celestial targets respectively. The initial states known by the module are the position $\boldsymbol{R}_{i/N}$ vector, velocity $\dot{\boldsymbol{R}}_{i/N}$ vector and acceleration $\ddot{\boldsymbol{R}}_{i/N}$ vector of the spacecraft and celestial bodies with respect to the inertial frame.

The normal vector $\boldsymbol{R}_n$ is perpenticular to the plane defined by the two celestial targets and the spacecraft location, and it is expressed as

$$\boldsymbol{R}_n = \boldsymbol{R}_{P_1/B} \times \boldsymbol{R}_{P_2/B} \tag{18}$$

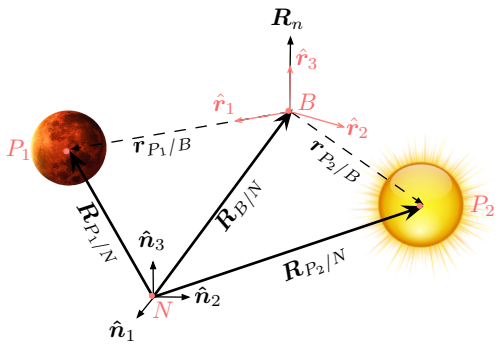

Figure 7: Illustration of a Constrained Celestial Two Body Pointing Scenario.

The desired base reference frame $\mathcal{R}$ is computed such that the first unit base vector $\hat{\boldsymbol{r}}_1$ points to the primary target. The third base vector $\hat{\boldsymbol{r}}_3$ is aligned with $\boldsymbol{R}_n$ while the last base vector $\hat{\boldsymbol{r}}_2$ completes the right-handed triplet.

$$\hat{\boldsymbol{r}}_1 = \frac{\boldsymbol{R}_{P_1/B}}{|\boldsymbol{R}_{P_1/B}|} \tag{19a}$$

$$\hat{\boldsymbol{r}}_3 = \frac{\boldsymbol{R}_n}{|\boldsymbol{R}_n|} \tag{19b}$$

$$\hat{\boldsymbol{r}}_2 = \hat{\boldsymbol{r}}_3 \times \hat{\boldsymbol{r}}_1 \tag{19c}$$

The celestial object locations relative to the spacecraft are found through

$$\boldsymbol{R}_{P_1/B} = \boldsymbol{R}_{P_1/N} - \boldsymbol{R}_{B/N} \tag{20a}$$

$$\boldsymbol{R}_{P_2/B} = \boldsymbol{R}_{P_2/N} - \boldsymbol{R}_{B/N} \tag{20b}$$

$$\tag{20c}$$

This setup aligns $\hat{\boldsymbol{b}}_2$ as closely as possible with $\boldsymbol{R}_{P_2/B}$. However, for general configurations it is not not possible to align these vectors perfectly while meeting the primary constraint at the same time.

The DCM that maps from the inertial frame $\mathcal{N}$ to the desired reference frame $\mathcal{R}$ is given by:

$$[RN] = \begin{bmatrix} {}^{\mathcal{N}}\hat{\boldsymbol{r}}_1^T \\ {}^{\mathcal{N}}\hat{\boldsymbol{r}}_2^T \\ {}^{\mathcal{N}}\hat{\boldsymbol{r}}_3^T \end{bmatrix} \tag{21}$$

The desired MRP attitude set $\boldsymbol{\sigma}_{R/N}$ is derived from $[RN]$.[8]

The angular velocity $\boldsymbol{\omega}_{R/N}$ and acceleration $\dot{\boldsymbol{\omega}}_{R/N}$ still need to be computed. In order to do so, the time derivatives of the reference base vectors are needed. The following expressions are found for the first inertial time derivatives:

$$\dot{\hat{\boldsymbol{r}}}_1 = ([I_{3\times3}] - \hat{\boldsymbol{r}}_1\hat{\boldsymbol{r}}_1^T)\frac{\dot{\boldsymbol{R}}_{P_1/B}}{|\boldsymbol{R}_{P_1/B}|} \tag{22a}$$

$$\dot{\hat{\boldsymbol{r}}}_3 = ([I_{3\times3}] - \hat{\boldsymbol{r}}_3\hat{\boldsymbol{r}}_3^T)\frac{\dot{\boldsymbol{R}}_n}{|\boldsymbol{R}_n|} \tag{22b}$$

$$\dot{\hat{\boldsymbol{r}}}_2 = \dot{\hat{\boldsymbol{r}}}_3 \times \boldsymbol{r}_1 + \boldsymbol{r}_n \times \dot{\hat{\boldsymbol{r}}}_3 \tag{22c}$$

where the inertial time derivatives of $\boldsymbol{R}_n$ are

$$\dot{\boldsymbol{R}}_n = \dot{\boldsymbol{R}}_{P_1/B} \times \boldsymbol{R}_{P_2/B} + \boldsymbol{R}_{P_1/B} \times \dot{\boldsymbol{R}}_{P_2/B} \tag{23}$$

$$\ddot{\boldsymbol{R}}_n = \ddot{\boldsymbol{R}}_{P_1/B} \times \boldsymbol{R}_{P_2/B} + 2\dot{\boldsymbol{R}}_{P_1/B} \times \dot{\boldsymbol{R}}_{P_2/B} + \boldsymbol{R}_{P_1/B} \times \ddot{\boldsymbol{R}}_{P_2/B} \tag{24}$$

Differentiating the unit vectors in Eqs. (22) yields:

$$\ddot{\hat{\boldsymbol{r}}}_1 = \frac{1}{|\boldsymbol{R}_{P_1/B}|}(([I_{3\times3}] - \hat{\boldsymbol{r}}_1\hat{\boldsymbol{r}}_1^T)\ddot{\boldsymbol{R}}_{P_1/B} - 2\dot{\hat{\boldsymbol{r}}}_1(\hat{\boldsymbol{r}}_1 \cdot \dot{\boldsymbol{R}}_{P_1/B}) - \hat{\boldsymbol{r}}_1(\dot{\hat{\boldsymbol{r}}}_1 \cdot \dot{\boldsymbol{R}}_{P_1/B})) \tag{25a}$$

$$\ddot{\hat{\boldsymbol{r}}}_3 = \frac{1}{|\boldsymbol{R}_n|}(([I_{3\times3}] - \hat{\boldsymbol{r}}_3\hat{\boldsymbol{r}}_3^T)\ddot{\boldsymbol{R}}_n - 2\dot{\hat{\boldsymbol{r}}}_3(\hat{\boldsymbol{r}}_3 \cdot \dot{\boldsymbol{R}}_n) - \hat{\boldsymbol{r}}_3(\dot{\hat{\boldsymbol{r}}}_3 \cdot \dot{\boldsymbol{R}}_n)) \tag{25b}$$

$$\ddot{\hat{\boldsymbol{r}}}_2 = \ddot{\hat{\boldsymbol{r}}}_3 \times \boldsymbol{r}_1 + \boldsymbol{r}_n \times \ddot{\hat{\boldsymbol{r}}}_3 + 2\dot{\hat{\boldsymbol{r}}}_3 \cdot \dot{\hat{\boldsymbol{r}}}_1 \tag{25c}$$

The reference angular rate is expressed in reference frame components as:

$${}^{\mathcal{R}}\boldsymbol{\omega}_{R/N} = {}^{\mathcal{R}}\begin{bmatrix} \boldsymbol{\omega}_{R/N} \cdot \hat{\boldsymbol{r}}_1 \\ \boldsymbol{\omega}_{R/N} \cdot \hat{\boldsymbol{r}}_2 \\ \boldsymbol{\omega}_{R/N} \cdot \hat{\boldsymbol{r}}_3 \end{bmatrix} = {}^{\mathcal{R}}\begin{bmatrix} \hat{\boldsymbol{r}}_3 \cdot \dot{\hat{\boldsymbol{r}}}_2 \\ \hat{\boldsymbol{r}}_1 \cdot \dot{\hat{\boldsymbol{r}}}_3 \\ \hat{\boldsymbol{r}}_2 \cdot \dot{\hat{\boldsymbol{r}}}_1 \end{bmatrix} \tag{26}$$

Taking the inertial derivative of Eq. (26) yields

$${}^{\mathcal{R}}\dot{\boldsymbol{\omega}}_{R/N} = {}^{\mathcal{R}}\begin{bmatrix} \dot{\boldsymbol{\omega}}_{R/N} \cdot \hat{\boldsymbol{r}}_1 \\ \dot{\boldsymbol{\omega}}_{R/N} \cdot \hat{\boldsymbol{r}}_2 \\ \dot{\boldsymbol{\omega}}_{R/N} \cdot \hat{\boldsymbol{r}}_3 \end{bmatrix} = {}^{\mathcal{R}}\begin{bmatrix} \dot{\hat{\boldsymbol{r}}}_3 \cdot \dot{\hat{\boldsymbol{r}}}_2 + \hat{\boldsymbol{r}}_3 \cdot \ddot{\hat{\boldsymbol{r}}}_2 - \boldsymbol{\omega}_{R/N} \cdot \dot{\hat{\boldsymbol{r}}}_1 \\ \dot{\hat{\boldsymbol{r}}}_1 \cdot \dot{\hat{\boldsymbol{r}}}_3 + \hat{\boldsymbol{r}}_1 \cdot \ddot{\hat{\boldsymbol{r}}}_3 - \boldsymbol{\omega}_{R/N} \cdot \dot{\hat{\boldsymbol{r}}}_2 \\ \dot{\hat{\boldsymbol{r}}}_2 \cdot \dot{\hat{\boldsymbol{r}}}_1 + \hat{\boldsymbol{r}}_2 \cdot \ddot{\hat{\boldsymbol{r}}}_1 - \boldsymbol{\omega}_{R/N} \cdot \dot{\hat{\boldsymbol{r}}}_3 \end{bmatrix} \tag{27}$$

V Dynamic Reference Modules

Next modules that generate a dynamic reference frame are considered. Here desired rotational motions are superimposed on the base reference frame $\mathcal{R}_0$. Very different behaviors like fixed-axis spinning, scientific scanning or orbit axis rotation can be pursued depending on the nature of the base reference and the requested rates.

V.A Fixed-Axis Spinning Relative to Base Reference Frame

A fixed-axis spinning motion is performed relative to the prior module output reference. Figure 8 shows the base pointing frame $\mathcal{R}_0 : \{\hat{\boldsymbol{r}}_{0,1}, \hat{\boldsymbol{r}}_{0,2}, \hat{\boldsymbol{r}}_{0,3}\}$ and the $\mathcal{R}_0$-frame fixed spinning vector $\boldsymbol{\omega}_{R/R_0}$. Here the $\boldsymbol{\omega}_{R/R_0}$ vector is, by definition of fixed spinning axis, aligned with the principal axis between the $\mathcal{R}$ and $\mathcal{R}_0$ frames. Thus

$$^{\mathcal{R}_0}\boldsymbol{\omega}_{R/R_0} \equiv {}^{\mathcal{R}}\boldsymbol{\omega}_{R/R_0} \tag{28}$$

The $\mathcal{R}$-frame constant spin vector in reference frame components ${}^{\mathcal{R}}\boldsymbol{\omega}_{R/R_0}$ is set as part of the module's configuration data.

At time $t = 0$, the reference attitude $\mathcal{R}$ relative to $\mathcal{R}_0$ is simply

$$\boldsymbol{\sigma}_{R/R_0}(t = 0) = \mathbf{0} \tag{29}$$

For any time $t > 0$, the current attitude is integrated using the associated MRP differential kinematic equations[16]

$$\dot{\boldsymbol{\sigma}}_{R/R_0} = \frac{1}{4}([I_{3\times3}](1 - |\boldsymbol{\sigma}_{R/R_0}|^2) + 2[\tilde{\boldsymbol{\sigma}}_{R/R_0}] + 2\boldsymbol{\sigma}_{R/R_0}\boldsymbol{\sigma}_{R/_0}^T)\ {}^{\mathcal{R}}\boldsymbol{\omega}_{R/R_0} \tag{30}$$

For example, using the Euler integration scheme yields

$$\boldsymbol{\sigma}_{R/R_0}(t) = \boldsymbol{\sigma}_{R/R_0}(t_{\text{previous}}) + \dot{\boldsymbol{\sigma}}_{R/R_0}\delta t \tag{31}$$

where

$$\delta t = t - t_{\text{previous}}$$

The final orientation of $\mathcal{R}$ relative to $\mathcal{N}$ is

$$[RN] = [RR_0(\boldsymbol{\sigma}_{R/R_0})][R_0N(\boldsymbol{\sigma}_{R_0/N})] \tag{32}$$

from which the required final reference attitude is extracted using standard DCM to MRP mapping $[RN] \to \boldsymbol{\sigma}_{R/N}$.

Next the angular velocity vector $\boldsymbol{\omega}_{R/N}$ and its derivative $\dot{\boldsymbol{\omega}}_{R/N}$ are developed. The angular velocity is defined as:

$$\boldsymbol{\omega}_{R/N} = \boldsymbol{\omega}_{R/R_0} + \boldsymbol{\omega}_{R_0/N} \tag{33}$$

where $\boldsymbol{\omega}_{R_0/N}(t)$ is the angular velocity of the base reference frame.

The angular acceleration of the $\mathcal{R}$ reference is computed by taking the inertial derivative of Eq. (33). The short hand dot notation is used to denote an inertial derivative of a vector.

$$\dot{\boldsymbol{\omega}}_{R/N} = \dot{\boldsymbol{\omega}}_{R/R_0} + \dot{\boldsymbol{\omega}}_{R_0/N} \tag{34}$$

The inertial derivative of the spinning vector $\boldsymbol{\omega}_{R/R_0}$ is evaluated using the transport theorem[8] to be

$$\frac{^{\mathcal{N}}\mathrm{d}}{\mathrm{d}t}(\boldsymbol{\omega}_{R/R_0}) = \frac{^{\mathcal{R}}\mathrm{d}}{\mathrm{d}t}(\boldsymbol{\omega}_{R/R_0}) + \boldsymbol{\omega}_{R/N} \times \boldsymbol{\omega}_{R/R_0} \tag{35}$$

Taking into account that $\boldsymbol{\omega}_{R/R_0}$ is constant as seen by the $\mathcal{R}$ reference frame and simplifying the cross product in Eq. (35), the following expression is found:

$$\dot{\boldsymbol{\omega}}_{R/N} = \boldsymbol{\omega}_{R_0/N} \times \boldsymbol{\omega}_{R/R_0} + \dot{\boldsymbol{\omega}}_{R_0/N} \tag{36}$$

Note that Eq. (36) is a vector expression, independent of any particular coordinate frame with respect to which vector components are taken. When evaluating Eq. (36) in the standard matrix form, naturally all vector components must be rotated to the same frame.

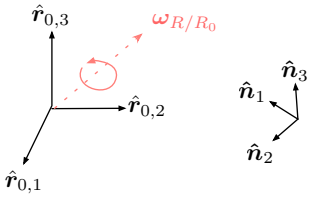

Figure 8: Illustration of a 3D Spinning Motion Inertial to the Base Reference $\mathcal{R}_0$

V.B Scanning and Spinning using Constant Euler 3-2-1 Angle Rates

V.B.1 General Algorithm

This dynamic module is able to achieve complex scanning maneuvers relative to the base reference frame using elegantly simple constant Euler angle rates. The module shown uses a 3-2-1 sequence, but naturally other Euler angle sequences could be considered. Simpler maneuvers like relative spinning about one of the reference frame axis are also possible.

Euler angles are often avoided in guidance algorithms because of their mathematical singularities. Yet, there are some guidance instances, such as relative scanning and spinning motions, where the advantages of the Euler set can be exploited in a robust and safe manner that is free of numerical issues. As a matter of fact, each set of Euler angles has a geometric singularity where two angles are not uniquely defined. Such geometric singularities result in mathematical singularities in the differential kinematic equations (always due to the second Euler angle). The key point is that these singularities only appear in the mapping from angular rates to Euler angle rates. In the present development, the inverse mapping takes place, which is free of singularities. Any geometric singularity would be inevitably reflected in Eq. (40).

An initial 3-2-1 Euler angle orientation $\boldsymbol{\theta}_{R/R0}$ and a constant set of rates $\dot{\boldsymbol{\theta}}_{R/R0}$ are defined as inputs to this dynamic module.

$$\boldsymbol{\theta}_{R/R_0} : \{\psi_0, \theta_0, \phi_0\}$$
$$\dot{\boldsymbol{\theta}}_{R/R_0} : \{\dot{\psi}, \dot{\theta}, \dot{\phi}\}$$

As this module considers constant Euler angle rates, the associated differential kinematic equations are integrable. The current Euler angles are thus expressed as

$$\psi(t) = \psi_0 + \dot{\psi}\delta t \tag{37a}$$
$$\theta(t) = \theta_0 + \dot{\theta}\delta t \tag{37b}$$
$$\phi(t) = \phi_0 + \dot{\phi}\delta t \tag{37c}$$

The time-varying desired reference attitude $[RN]$ is evaluated by adding the dynamic attitude $[RR_0]$ onto the base reference attitude $[R_0N]$:

$$[RN] = [RR_0(\psi(t), \theta(t), \phi(t))][R_0N(\boldsymbol{\sigma}_{R_0/N})] \tag{38}$$

The output orientation of this dynamic module is obtained by converting the $[RN]$ matrix into the equivalent MRP coordinates

$$[RN] \rightarrow \boldsymbol{\sigma}_{R/N} \tag{39}$$

The matrix ${}^{\mathcal{R}}\boldsymbol{\omega}_{R/R_0}$ is obtained from the 3-2-1 Euler angle differential kinematic equations:

$${}^{\mathcal{R}}\boldsymbol{\omega}_{R/R_0} = \begin{bmatrix} -\sin\theta & 0 & 1 \\ \sin\phi\cos\theta & \cos\phi & 0 \\ \cos\phi\cos\theta & -\sin\phi & 0 \end{bmatrix} \begin{bmatrix} \dot{\psi} \\ \dot{\theta} \\ \dot{\phi} \end{bmatrix} \tag{40}$$

Substituting this expression into Eq. (33) yields the output state $\boldsymbol{\omega}_{R/N}$.

To determine the output reference frame angular acceleration, the $\mathcal{R}$-frame derivative of $\boldsymbol{\omega}_{R/R_0}$ is considered first. Making use of the Euler angle rates being constant, this derivative is

$$\frac{{}^{\mathcal{R}}\mathrm{d}}{\mathrm{d}t}(\boldsymbol{\omega}_{R/R_0}) = {}^{\mathcal{R}}\begin{bmatrix} -\dot{\theta}\dot{\psi}\cos\theta \\ (\dot{\phi}\cos\phi\cos\theta - \dot{\theta}\sin\phi\sin\theta)\dot{\psi} - \dot{\phi}\dot{\theta}\sin\phi \\ -(\dot{\phi}\sin\phi\cos\theta + \dot{\theta}\cos\phi\cos\theta)\dot{\psi} - \dot{\phi}\dot{\theta}\cos\phi \end{bmatrix} \tag{41}$$

Following Eq. (35), the angular acceleration is

$$\dot{\boldsymbol{\omega}}_{R/N} = \frac{^{\mathcal{R}}\mathrm{d}}{\mathrm{d}t}(\boldsymbol{\omega}_{R/R_0}) + \boldsymbol{\omega}_{R_0/N} \times \boldsymbol{\omega}_{R/R_0} + \dot{\boldsymbol{\omega}}_{R_0/N} \tag{42}$$

V.B.2 Orbit Axis Spinning

Spinning about an orbit axis is achieved by applying a single axis rotation of the 3-2-1 Euler angle set onto a base reference. Both Hill and velocity frames are presented as base reference orbit frames. The simple spin modes are achieved using the following 3-2-1 Euler angel rates:

$$\{\dot{\psi}, 0, 0\} = \text{ Spinning motion about the third axis of the orbit frame, i.e. angular momentum direction } \hat{\boldsymbol{\imath}}_h$$
$$\{0, \dot{\theta}, 0\} = \text{ Spinning motion about the second axis of the orbit frame}$$
$$\{0, 0, \dot{\phi}\} = \text{ Spinning motion about the first axis of the orbit frame}$$

Figure 9 illustrates a spinning motion of rate $\dot{\phi}$ about the nadir axis of the Hill frame $\hat{\boldsymbol{\imath}}_r$. In this case the base orbit frame is the Hill frame:

$$\mathcal{R}_0 : \{\hat{\boldsymbol{r}}_{0,1}, \hat{\boldsymbol{r}}_{0,2}, \hat{\boldsymbol{r}}_{0,3}\} \equiv \mathcal{H} : \{\hat{\boldsymbol{\imath}}_r, \hat{\boldsymbol{\imath}}_\theta, \hat{\boldsymbol{\imath}}_h\}$$

and the Euler angle rates are defined as:

$$\dot{\boldsymbol{\theta}}_{R/R0} = \{0, 0, \dot{\phi}\}$$

V.B.3 Axis Scanning

Scanning rasters are performed through the consecutive request of Euler angle offsets and rates. The use of the 3-2-1 Euler set in particular facilitates a wide range of scanning patterns. For example, Fig. 10 illustrates two scanning patterns consisting of several rasters. The scanning is performed relative to the time-varying base reference frame $\mathcal{R}_0 : \{\hat{\boldsymbol{r}}_{0,1}, \hat{\boldsymbol{r}}_{0,2}, \hat{\boldsymbol{r}}_{0,3}\}$. The continuous lines correspond to the nominal raster lines of scientific interest, while the dashed lines indicate the transition between one raster and the following. Each nominal line is defined by a specific offset $\boldsymbol{\theta}_{R/R0} : \{\psi_0, \theta_0, \phi_0\}$ and angle rate $\dot{\boldsymbol{\theta}}_{R/R0} : \{\dot{\psi}, \dot{\theta}, \dot{\phi}\}$. The scan pattern in Fig. 10(a) is achieved through constant θ_0 and ψ_0 offset values and a linearly time varying ψ angle. The asterisk scanning pattern in Fig. 10(b) is achieved through initial offsets in both ψ and θ, and allowing both angles to have constant rates.

In order to complete complex scanning patterns that combine multiple maneuvers, the Euler angle rotation module is complemented with a higher-level module called raster manager. The function of the raster manager is to request the appropriate Euler angle offsets and rates at the configured raster times. The numerical simulations section demonstrates how these scanning patterns are achieved by staging multiple reference frame modules.

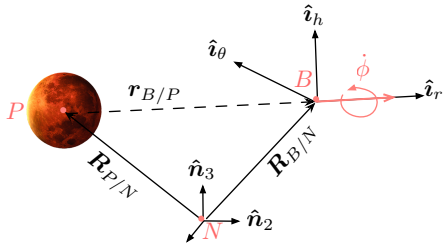

Figure 9: Hill Frame Nadir Axis Spinning.

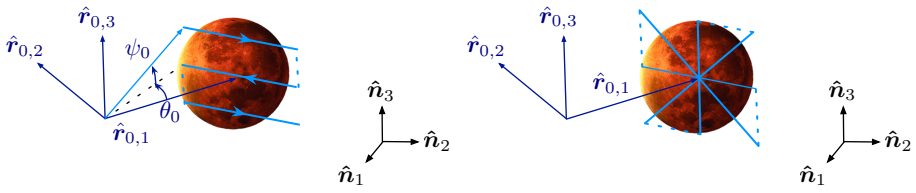

a) Rectangular Raster Maneuver. **b)** Asterisk Raster Maneuver.

Figure 10: Scientific Scanning Patterns.

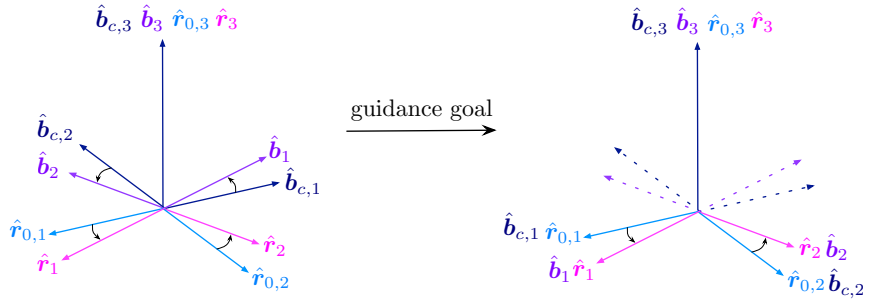

Figure 11: Simplified Fixed Axis Rotation Scenario to Illustrate the $\mathcal{B}$ to Control Body $\mathcal{B}_c$ Frames Relationship.

VI Tracking Error Module

This section considers the following scenario. What if the high-gain antenna unit direction vector is to be reoriented and it is not lined up with the primary body frame base vector. One option is to map the vector components and inertia tensor in the control formulation to this new body-fixed frame. However, this is not a convenient operation to implement digitally. The following approach allows the same body-fixed frame $\mathcal{B}$ to be used while simply adjusting the reference orientation. In this scenario the control should not drive the primary $\mathcal{B}$ to the computed reference frame (labeled $\mathcal{R}_0$ in this section as it is the input to the tracking error module). Rather, an alternate control body fixed-frame $\mathcal{B}_c$ that is aligned with the antenna body frame must be driven towards the input reference frame. Thus, as $\mathcal{B}_c \to \mathcal{R}_0$ then $\mathcal{B} \to \mathcal{R}$ if

$$[B_cB] = [R_0R] \tag{43}$$

as illustrated in Figure 11. The control body-frame $\mathcal{B}_c$ could correspond to any body-fixed frame that differs from $\mathcal{B}$ by a constant angular offset $[B_cB]$.

The attitude tracking error module receives the main body frame orientation $[BN(\boldsymbol{\sigma}_{B/N})]$ from navigation. Further, the constant body to control-body DCM $[B_cB]$ is set within the module. The input reference frame DCM $[R_0N(\boldsymbol{\sigma}_{R_0/N})]$ has been computed by the base pointing and dynamic modules.

The orientation of the final reference frame $\mathcal{R}$ is defined relative to the inertial frame by subtracting the body-frame from the input reference orientation:

$$[RN] = [RR_0][R_0N] = [B_cB]^T[R_0N] \tag{44}$$

With the discussed generalization, it is possible to correct any sensor or component frame orientation using the same classical tracking error algorithms that deal with the main body frame. The need of creating particular code for the guidance of different spacecraft-fixed frames is overcome.

Next the attitude tracking error $\boldsymbol{\sigma}_{B/R}$ and angular velocity error ${}^{\mathcal{B}}\boldsymbol{\omega}_{B/R}$ are derived. The attitude error of $\mathcal{B}$ relative to the $\mathcal{R}$ reference frame is

$$[BR(\boldsymbol{\sigma}_{B/R})] = [BN(\boldsymbol{\sigma}_{B/N})][RN(\boldsymbol{\sigma}_{R/N})]^T \tag{45}$$

The MRP set $\boldsymbol{\sigma}_{B/R}$ is readily obtained from $[BR]$.[8]

The rate tracking error is defined as

$$\boldsymbol{\omega}_{B/R} = \boldsymbol{\omega}_{B/N} - \boldsymbol{\omega}_{R/N} = \boldsymbol{\omega}_{B/N} - \boldsymbol{\omega}_{R_0/N} \tag{46}$$

because $[B_cB]$ is a constant attitude correction and $\boldsymbol{\omega}_{R/R_0} = \mathbf{0}$.

VII Numerical Simulations

VII.A Numerical Scenario Common Setup

The rigid body equations of motion in Eq. (1) are numerically simulated in Basilisk to validate and illustrate the performance of the presented reference frame modules. The orientation is controlled through a set of four RWs. The dynamic states are integrated using a Range-Kutta 4 scheme running at 10 Hz. The MRP feedback control in Eq. (4) is used to drive the spacecraft orientation towards the desired reference motion. The simulated navigation data $\boldsymbol{\sigma}_{B/N}$ and $\boldsymbol{\omega}_{B/N}$ is without any sensor corruptions to better illustrate that the control law does achieve asymptotic tracking of the reference motion. Each simulation has a maneuver duration of 9600 seconds (≈ 2.7 hours). The orbital parameters of the simulated Mars orbit scenario are presented in Table 1 and the control related parameters are shown in Table 2.

Table 1: Initial Orbital Elements

Parameter	Value	Units
Semi-major Axis	$7471.618 (\approx 2.2 R_{\text{Mars}})$	km
Eccentricity	0.4	
Inclination	0.0	deg
Longitude of Ascendant Node	0.0	deg
Argument of Perigee	0.0	deg
True Anomaly	270.0	deg

Table 2: Control and Spacecraft Parameters

Parameter	Value	Units
Attitude Error Gain K	2.531	$\frac{\text{kg}\cdot\text{m}^2}{\text{s}}$
Rate Error Gain P	45.0	$\frac{\text{kg}\cdot\text{m}^2}{\text{s}}$
$\hat{\boldsymbol{g}}_{s_1}$	$[-0.5, 0.5, -\frac{\sqrt{2}}{2}]$	
$\hat{\boldsymbol{g}}_{s_2}$	$[0.5, 0.5, -\frac{\sqrt{2}}{2}]$	
$\hat{\boldsymbol{g}}_{s_3}$	$[0.5, -0.5, -\frac{\sqrt{2}}{2}]$	
$\hat{\boldsymbol{g}}_{s_4}$	$[-0.5, -0.5, -\frac{\sqrt{2}}{2}]$	
J_{s_i}	0.1591549	$\text{kg}\cdot\text{m}^2$
I_1, I_2	700	$\text{kg}\cdot\text{m}^2$
I_3	800.0	$\text{kg}\cdot\text{m}^2$

The spacecraft is flying through the periapses region on a highly eccentric orbit. Consequently, there is a considerably amount of variability on the spacecraft orbit rates. In the first control scenario, asymptotically tracking this orbital motion emphasizes the challenges of properly evaluating acceleration and rates.

With the chosen proportional gain P, the control time decay constant[8] is $\tau \approx 30$ sec. The K gain is computed to yield a critically damped system. This choice of gains provides a non-aggressive control response. Although initial big torque requests are unavoidable, operating with non-saturated reaction wheels is guaranteed for the rest of the simulated maneuver.

VII.B Orbit Axis Rotation

The first simulation illustrates a guidance solution that has the spacecraft line up with the Hill frame and applies an offset attitude given by a 180 degree rotation about the third body axis $\hat{\boldsymbol{b}}_3$. The resulting frame points the first principal axis of the spacecraft body $\hat{\boldsymbol{b}}_1$ towards the planet. Hence, $\hat{\boldsymbol{b}}_1$ becomes antiparallel to the first axis of the Hill frame $\hat{\boldsymbol{i}}_r$. Superimposed on this base reference motion there is a spinning motion about $\hat{\boldsymbol{i}}_r$. Here $\hat{\boldsymbol{b}}_1$ remains fix while $\hat{\boldsymbol{b}}_2$ and $\hat{\boldsymbol{b}}_3$ rotate in the local-horizontal orbit plane. A screen capture of the Graphical User Interface (GUI) used to visualize the guidance motion is shown in Fig. 13. Figure 12 shows the guidance stack to achieve the suggested spinning maneuver about the nadir direction of the orbit.

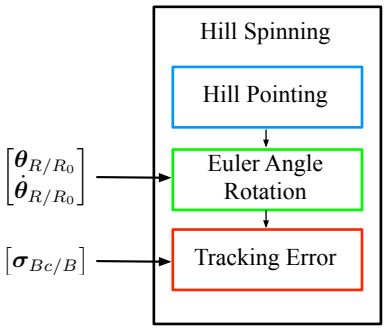

Figure 12: Hill Spinning Stack.

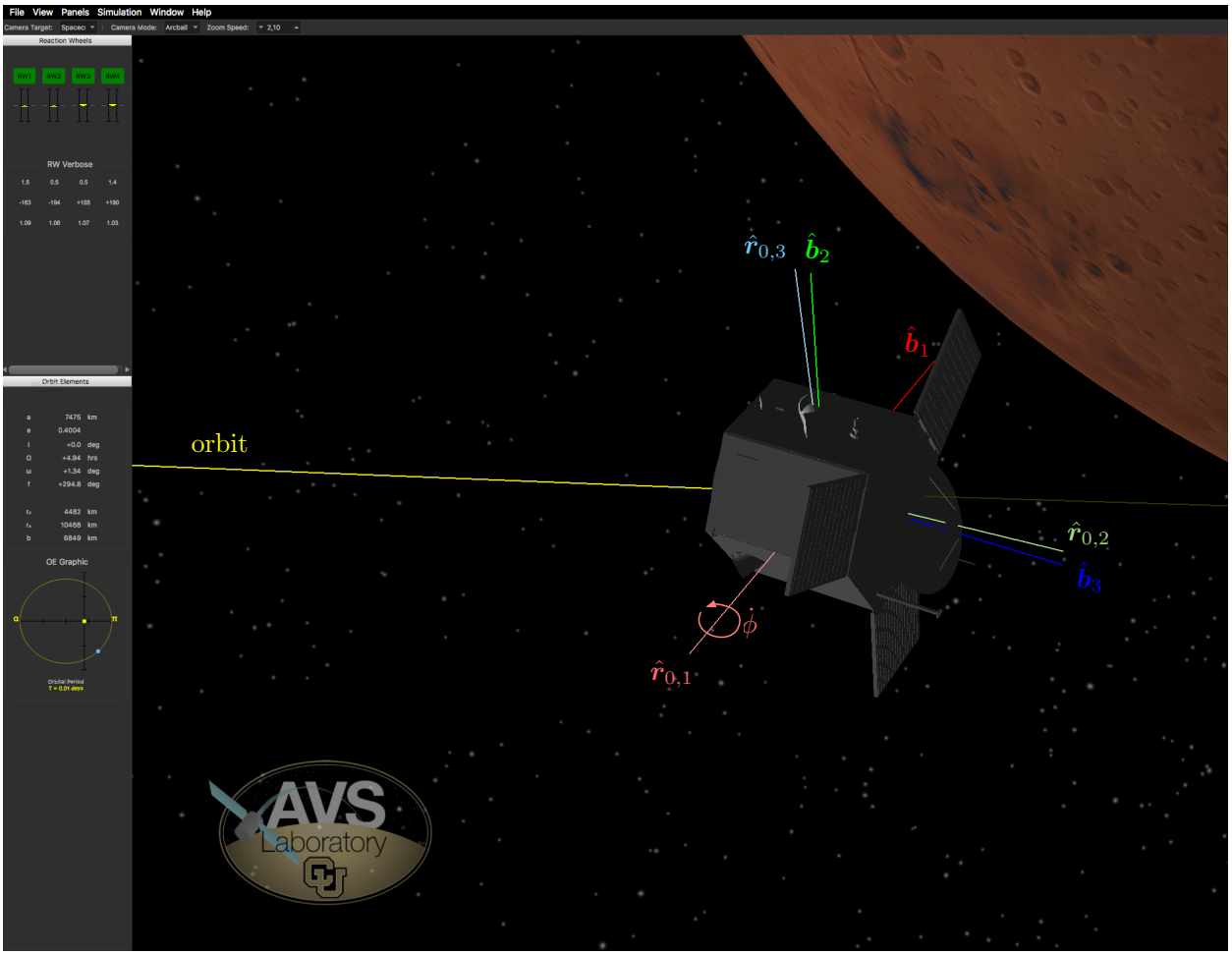

Figure 13: Basilisk Visualization of a Nadir Spinning Maneuver.

Table 3: Euler Angle Rotation Configuration Data.

Parameter	Value	Units	Description
$\boldsymbol{\theta}_{R/R_0} : \{\psi, \theta, \phi\}$	$[0.0, 0.0, 0.0]$	deg/s	Initial 3-2-1 set of Euler angle set relative to the base reference $\mathcal{R}_0$.
$\dot{\boldsymbol{\theta}}_{R/R_0} : \{\dot{\psi}, \dot{\theta}, \dot{\phi}\}$	$[0.0, 0.0, 0.3]$	deg/s	Desired 3-2-1 set of Euler angle rates relative to the base reference $\mathcal{R}_0$.

The configuration parameter of the tracking error module $\boldsymbol{\sigma}_{B_c/B}$ is the control body-frame correction

$$\boldsymbol{\sigma}_{Bc/B} = [0.0, 0.0, 1.0] \tag{47}$$

which yields the 180 degree offset in the orbit plane. The configuration data of the Euler angle rotation module is provided in Table 3.

Figure 14 shows the reference attitude sets generated at each stage. Figure 14(a) shows the time varying Hill-frame orientation, denoted $\mathcal{R}_0$ in this scenario. The rapid orientation change is due to the spacecraft flying through periapses on a highly elliptic orbit. The constant Euler angle rates in Fig. 14(b) show that only $\dot{\phi} \neq 0$. Cascading these two reference frames finally yields the complex reference frame motion shown in Fig. 14(c). Fig. 15 displays the final attitude and rate tracking errors as well as the applied control torque. For visualization purposes, these latter plots only show results for half of the simulation time. At this point in time the motion is already stabilized. The body frame aligns asymptotically with the desired reference frame, illustrating the proper kinematic addition of the base and dynamic reference frames, as well as the correction of the body frame to control body frame. The control torque

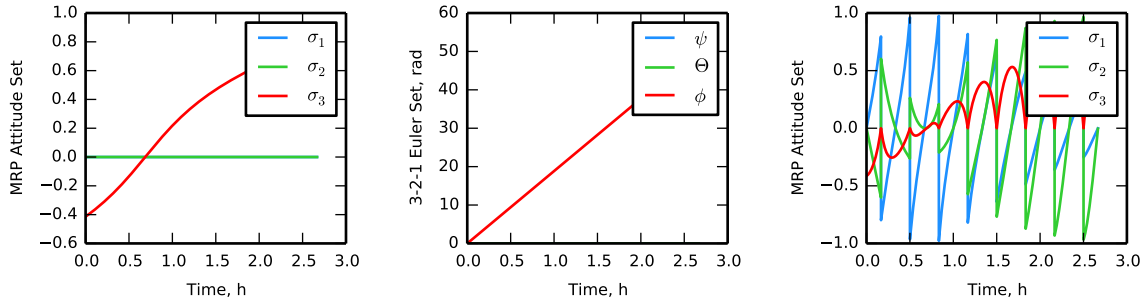

a) Base reference MRP $\boldsymbol{\sigma}_{R0/N}$. **b)** 3-2-1 Euler set $\boldsymbol{\theta}_{R0/R}$. **c)** Desired reference MRP $\boldsymbol{\sigma}_{R/N}$.

Figure 14: Generated Attitude Sets.

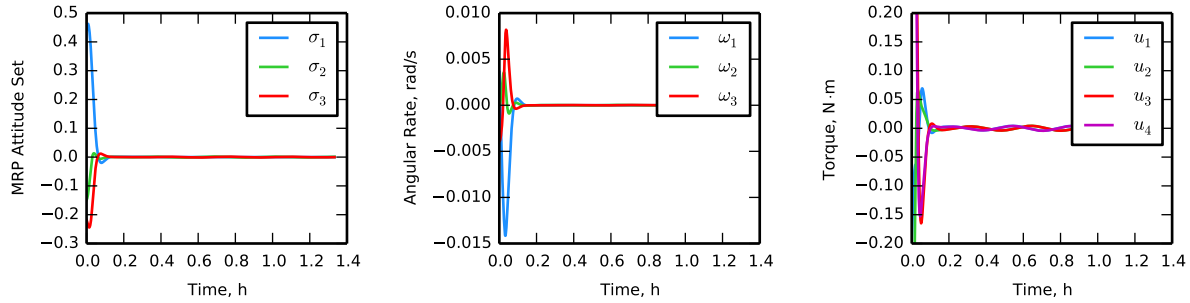

a) Attitude tracking error $\boldsymbol{\sigma}_{B/R}$. **b)** Rate tracking error $\boldsymbol{\omega}_{B/R}$. **c)** Applied control torque $\boldsymbol{u}$.

Figure 15: Tracking Errors and Control Torque.

in Fig. 15(c) is capped to a maximum RW torque of 0.2 N·m. Note that u_i correspond to the torque of each reaction wheel. It is shown that saturation only takes place at the very beginning of the maneuver. Performing a nadir axis spinning is an unnatural, i.e. non-equilibrium, motion. Hence, it is expected that the reference torques do not converge to zero.

VII.C Raster Maneuver

The second simulation performs a scanning maneuver to achieve an asterisk pattern across an inertial reference like the one illustrated in Fig. 10(b). The guidance stack for the multi-raster scanning motion is depicted in Fig. 16. Note that in this simulation, a raster manager module is attached to the Euler rotation module. The raster manager commands a sequence of Euler angle offsets and rates at the configured raster times. Each raster lasts for 1600 seconds (≈ 0.45 hours). The resulting complex reference motion is generated using only a total of $N = 4$ raster commands. Additionally, the spacecraft is smoothly driven back to the starting scanning point.

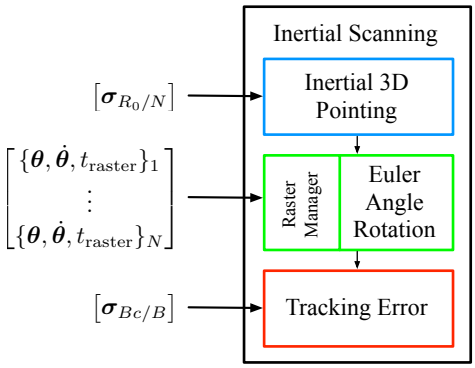

Figure 16: Inertial Scanning Stack.

Table 4: Raster Manager Configuration Data.

Parameter	Value	Units	Description
$\boldsymbol{\theta}_{R/R_0} : \{\psi, \theta, \phi\}_1$	$[\alpha, 0.0, 0.0]$	deg	Initial 3-2-1 Euler angle set of the first raster.
$\dot{\boldsymbol{\theta}}_{R/R_0} : \{\dot{\psi}, \dot{\theta}, \dot{\phi}\}_1$	$[-\dot{\alpha}, 0.0, 0.0]$	deg/s	3-2-1 Euler angle rates of the first raster.
$\boldsymbol{\theta}_{R/R_0} : \{\psi, \theta, \phi\}_2$	$[-\alpha, -\alpha, 0.0]$	deg	Initial 3-2-1 Euler angle set of the first raster.
$\dot{\boldsymbol{\theta}}_{R/R_0} : \{\dot{\psi}, \dot{\theta}, \dot{\phi}\}_2$	$[\dot{\alpha}, \dot{\alpha}, 0.0]$	deg/s	3-2-1 Euler angle rates of the second raster.
$\boldsymbol{\theta}_{R/R_0} : \{\psi, \theta, \phi\}_3$	$[\alpha, -\alpha, 0.0]$	deg	Initial 3-2-1 Euler angle set of the third raster.
$\dot{\boldsymbol{\theta}}_{R/R_0} : \{\dot{\psi}, \dot{\theta}, \dot{\phi}\}_3$	$[-\dot{\alpha}, \dot{\alpha}, 0.0]$	deg/s	3-2-1 Euler angle rates of the third raster.
$\boldsymbol{\theta}_{R/R_0} : \{\psi, \theta, \phi\}_4$	$[0.0, \alpha, 0.0]$	deg	Initial 3-2-1 Euler angle set of the forth raster.
$\dot{\boldsymbol{\theta}}_{R/R_0} : \{\dot{\psi}, \dot{\theta}, \dot{\phi}\}_4$	$[0.0, -\dot{\alpha}, 0.0]$	deg/s	3-2-1 Euler angle rates of the forth raster.
$t_{\text{raster, i}}$	1600	s	Time duration of each commanded raster maneuver.

The inertial pointing module and attitude tracking error module are initialized with the following parameters:

$$\boldsymbol{\sigma}_{R_0/N} = [0.0, 0.0, 0.0] \tag{48a}$$

$$\boldsymbol{\sigma}_{Bc/B} = [0.0, 0.0, 0.0] \tag{48b}$$

Thus, the requested inertial attitude is that of the global inertial frame with $\mathcal{R}_0 \equiv \mathcal{N}$. The control body frame coincides with the principal body frame through $\mathcal{B}_c \equiv \mathcal{B}$ or $[B_c B] = [I_{3\times3}]$.

The configuration parameters of the raster manager are provided in Table 4 where α and $\dot{\alpha}$ are defined as

$$\alpha = 8.0 \text{ deg} \tag{49}$$

$$\dot{\alpha} = \frac{2\alpha}{t_{\text{raster}}} \tag{50}$$

Figure 17 shows the evolution of the 3-2-1 Euler angle set while performing the several scan lines, as well as the attitude tracking error and rate error along the complete maneuver. Note that the peaks in the tracking error plots correspond to the command of a new raster line and are an expected behavior. Here, the spacecraft asymptotically transitions from its current raster line to the next.

Figure 18(a) compares the desired nominal raster lines with the actual yaw-pitch angles scanned in the maneuver. In order to get into the desired rasters on time, a small angle offset needed to be commanded, which is also depicted. The choice of the offset is a trade off with the picked control gains. In this case, an offset of 0.5α was found to work well for any value of α. This additional angular offset requires small adjustments on the raster time. The numbered points at the beginning and end of the scan lines indicate the order of the four rasters: points labeled with letter a correspond to the beginning of the nominal raster line, while points labeled with letter b correspond to the end. Each raster command takes the spacecraft from its current point b to a new initial attitude and rate corresponding to the next point a (transition). Note that from point $4(b)$, the spacecraft is driven back to the initial point where the scanning maneuver started, $1(a)$.

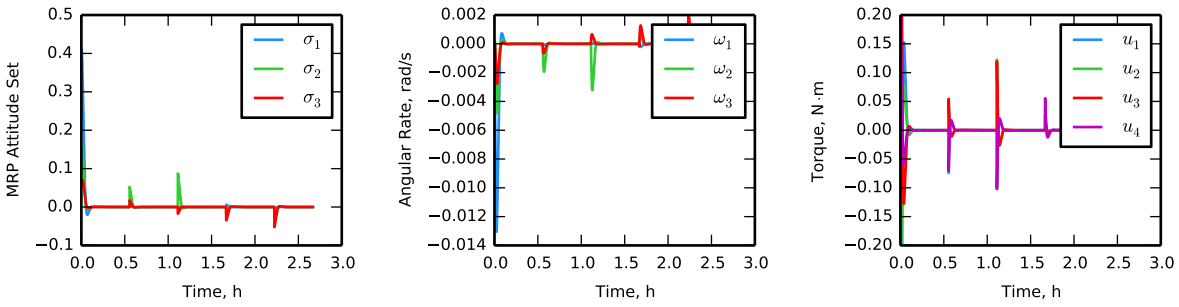

a) Attitude tracking error $\boldsymbol{\sigma}_{B/R}$. **b)** Rate tracking error $\boldsymbol{\omega}_{B/R}$. **c)** Applied control torque $\boldsymbol{u}$.

Figure 17: Tracking Errors and Control Torque.

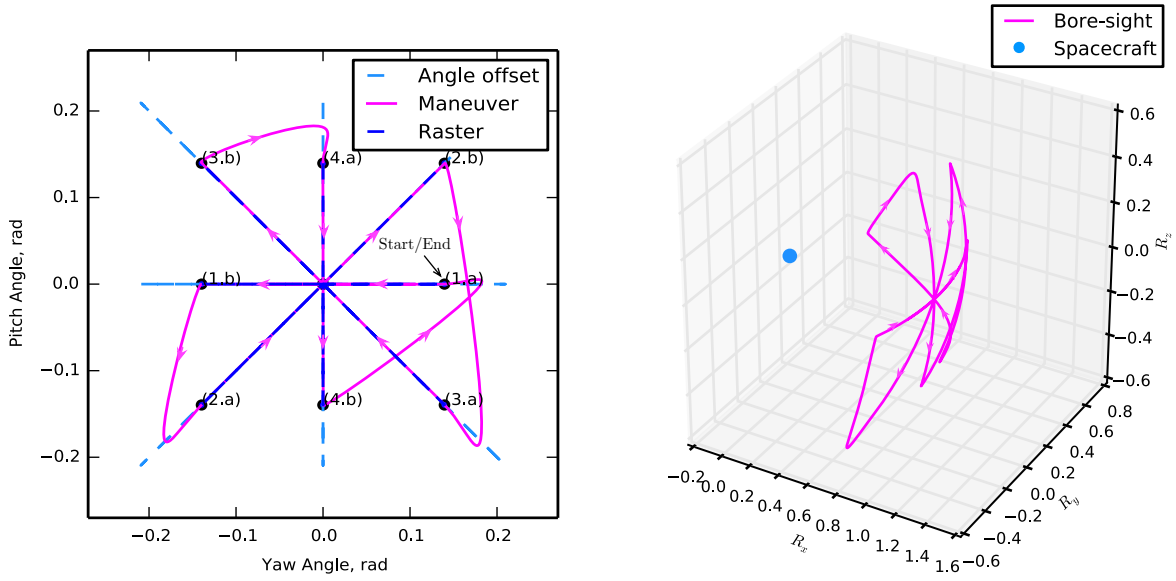

a) Nominal Rasters vs. Achieved Maneuver for $\alpha = 8$ deg.

b) Achieved 3D Bore-sight Pointing for $\alpha = 24$ deg.

Figure 18: Achieved Asterisk Scanning Pattern.

Figure 18(b) shows the three-dimensional view of the spacecraft's bore-sight pointing. Cartesian coordinates of the bore-sight pointing are represented in an analogous scanning maneuver of nominal angle $\alpha = 24$ degrees. The single blue dot corresponds to the position of the spacecraft, from which a scanning pattern is projected on a unit sphere.

VIII Conclusions

A novel reference generation architecture is presented where complex guidance is achieved through a set of atomic reference frame behaviors. A fundamental aspect is that the proposed guidance scheme is developed in a completely general way. Mission-specific needs can then be met by arranging the existing software in a reliable and systematical manner. Two types of generated references are distinguished. First, the base reference frame is generated using, if necessary, the satellite's orbit information. Next, dynamic reference frame behaviors are super-imposed to yield spinning or scanning maneuvers relative to the base reference frame. Alternate body-fixed frame alignments are accounted for during the tracking error computation. A key advantage of this approach is that each reference frame generation module can be tested and verified individually. This simplifies the overall ADCS validation approach as complex guidance functionality is achieved through combination of tested core modules. Numerical simulations validate that the generated reference motion exhibits the expected performance, and the associated feedforward control terms allow the spacecraft to asymptotically converge onto the reference motion.

References

[1]Lefferts, E. J., Markley, F. L., and Shuster, M. D., "Kalman Filtering for Spacecraft Attitude Estimation," *AIAA Journal of Guidance, Control, and Dynamics*, Vol. 5, No. 5, 1981, pp. 417–429.

[2]Crassidis, J. L. and Markley, F. L., "Survey of Nonlinear Attiude Estimation Methods," *AIAA Journal of Guidance, Control, and Dynamics*, Vol. 30, No. 1, 2007, pp. 12–28.

[3]Crassidis, J. L. and Markley, F. L., "Unscented Filtering for Spacecraft Attitude Estimation," *AIAA Journal of Guidance, Control, and Dynamics*, Vol. 26, No. 4, July–Aug. 2003, pp. 536–542.

[4]Karlgaard, C. D. and Schaub, H., "Nonsingular Attitude Filtering Using Modified Rodrigues Parameters," *Journal of the Astronautical Sciences*, Vol. 57, No. 4, Oct.–Dec. 2010, pp. 777–791, doi:10.1007/BF03321529.

[5]O'Keefe, S. A. and Schaub, H., "Shadow Set Considerations For Modified Rodrigues Parameter Attitude Filtering," *AIAA Journal of Guidance, Control, and Dynamics*, Vol. 37, No. 6, 2014, pp. 2030–2035, doi:10.2514/1.G000405.

[6]Bayard, D. S., "High-Precision Three-Axis Pointing and Control," *Encyclopedia of Aerospace Engineering*, edited by R. Blockey and W. Shyy, John Wiley & Sons, Chichester, UK, 2010, doi:10.1002/9780470686652.eae300.

[7]Tsiotras, P., Shen, H., and Hall, C. D., "Satellite Attitude Control and Power Tracking with Energy/Momentum Wheels," *Journal of Guidance, Control, and Dynamics*, Vol. 24, No. 1, 2001, pp. 23–34.

[8]Schaub, H. and Junkins, J. L., *Analytical Mechanics of Space Systems*, AIAA Education Series, Reston, VA, 3rd ed., 2014, doi:10.2514/4.102400.

[9]Wie, B., *Space Vehicle Dynamics and Control*, AIAA Education Series, Reston, VA, 2nd ed., 2008.

[10]Leveson, N. G., "The Role of Software in Spacecraft Accidents," *AIAA Journal of Spacecraft and Rockets*.

[11]de Lafontaine, J., Buijs, J., Vuilleumier, P., den Braembussche, P. V., and Mellab, K., "Development of the PROBA Attitude Control and Navigation Software," 2000.

[12]Schulte, P. Z. and Spencer, D. A., "Development of an Integrated Spacecraft Guidance, Navigation, And Control Subsystem for Automated Proximity Operations," October 2014.

[13]Wiener, T. F., *Theoretical Analysis of Gimballess Inertial Reference Equipment Using Delta-Modulated Instruments*, Ph.D. dissertation, Department of Aeronautics and Astronautics, Massachusetts Institute of Technology, Cambridge, MA, March 1962.

[14]Tsiotras, P. and Longuski, J. M., "A New Parameterization of the Attitude Kinematics," *Journal of the Astronautical Sciences*, Vol. 43, No. 3, 1996, pp. 243–262.

[15]Tanygin, S., "The Many TRIAD Algorithms," *AAS/AIAA Spaceflight Mechanics Meeting*, Sedona, AZ, Feb. 2007, Paper AAS 07-104.

[16]Shuster, M. D., "A Survey of Attitude Representations," *Journal of the Astronautical Sciences*, Vol. 41, No. 4, 1993, pp. 439–517.